Egyptian Journal of Chemistry

http://ejchem.journals.ekb.eg/

Nanocomposite of TiO₂ @ Ni- or Co-doped Graphene Oxide for Efficient Photocatalytic Water Splitting

Mohammad M. Almutairi[1,2], Ebraheim E. Ebraheim[2], Mohamed S. Mahmoud[2,3], Mohamed S. Atrees[4], Mohamed E.M. Ali[5*], Yasser M. Khawassek[4]
[1]Ministry of Electricity and Water, Kuwait, P.O.12010
[2]Chemical Engineering Department, Minia University, El-Minia, 61111, Egypt.
[3]Collage of Applied Science, Department of Engineering, Suhar, 331, Oman.
[4]Nuclear Materials Authority, Maadi Road, Elqattamia, Cairo, Egypt. P.O. 530.
[5]Water Pollution Research Department, Environmental Sciences Division, National Research Centre (NRC), Egypt, P.O. 12622.

NANOCOMPOSITES of TiO₂@Ni-doped or Co-doped graphene oxide (GO) have been sucessfully prepared and are employed for photocatalytic water splitting. TEM images showed doted nanostructure and scattered-appearance of Co, Ni with and TiO₂ nanoparticles on GO sheet. The XRD patterns proved the existence of the crystal planes of Ni, Co and TiO₂ nanoparticles on GO. Moreover, the absorption spectrum of the prepared samples showed a better percentage of absorption of the visible light upon introducing NiO or CoO. EDX analysis results confirmed the presence of Co, C, O, and Ti elements in the sample. Interestingly, both n-TiO₂/p-NiO/GO and n-TiO₂/p-CoO/GO heterojunctions photocatalysts improved the photo-catalytic activity for water splitting nonetheless with different mechanisms. The n-TiO₂/p-NiO/GO photocatalyst showed a higher hydrogen production rate of 0.3 mmole/min/g than that of n-TiO₂/p-CoO/GO. The generated e/h pairs in the TiO₂ part of the catalyst is kept through the effect of the electric field formed by the p-NiO/n-TiO₂ heterojunction while Co presence narrows the bandgap and promotes both hydrogen evolution reactions at the conduction and valence band of heterojunctions.

Keywords: Graphene oxide, TiO₂ nanoparticles, Photocatalyst, Water splitting.

Introduction

Hydrogen is usually considered as a clean form of energy. Recently, it received lots of attention in the energy market as an energy carrier [1]. The dominant production process of hydrogen includes fossil fuel as a precursor. Hydrogen as a fuel is admitted to the proton exchange membrane (PEM) fuel cell to generate electricity and water vapor with an efficiency of more than 70%. However, still the debates of storing and supplying the hydrogen hider it is widespread as an alternative energy carrier. Therefore, numerous researchers are investigating the components of the PEM fuel cell as well as the innovative routes for hydrogen production and storage. Alternatively, water is the most suitable and abundant source of hydrogen. Different ways, including water reduction, photocatalytic water splitting and water purification have been investigated [2,3]. Hitherto, intensive researches are devoted to the solar energy-based hydrogen production. In their midst, photocatalytic water splitting has received intense attention [4,5] due to the concentrated researches in nanostructured catalysts.

Typically, the activity of photocatalysts depend crystal size, shape, structure and modification. Metal desposition on TiO₂ is significantly enhanced photocatalytic activity when of titania due to the attraction of electrons to the metal particles on TiO₂ [6]. The incorporation of CoO on titanate nanotube enhances the activity of anatase under solar irradiation, the improvement proceeds

via preventing the recombination of hole-electron and modification band gap[7].

Another modification method is the coupling of TiO_2 with carbon materials. TiO_2 modified with carbon nanomaterials have been previously investigated for photocatalytic activity. It was previously proved that graphene and modified neodymium/GO incorporated with titania enhances the absorption ability and electron transfer rate of TiO_2 as well as shifting the absorption edge of TiO_2 to the visible-light region. Consequently, it is expected that the synergistic effect of incorporating GO with titania nanoparticles will promote the photo-catalytic reactions both at conduction and valence bands [8,9]. Moreover, graphene oxide (GO) is a potential photocatalytic material due to its excellent solubility, and tunable bandgap [10].

Herein, the effect of introducing Ni, and Co, to the lattice of GO, and incorporating with titania nanoparticles has been examined. The Ni sample will be denoted as n-TiO_2@p-NiO/GO while the Co samples will be denoted as n-TiO_2@p-CoO/GO henceforth. The effect of such incorporation on the photocatalytic activity towards water splitting under the visible light irradiation has also been investigated.

Experimental

Catalyst preparations:

In the preparation step, all the chemicals are obtained from the Sigma Aldrich Co. (UK) and used without further modification. A mixture of H_3PO_4/H_2SO_4 with mass ratio 9/1 respectively was added to a mixture of two grams of graphite powder and one gram of $NaNO_3$. The reaction beaker is placed in an ice bath with stirring to control the temperature below 20 °C. Then, slowly 12 g of $KMnO_4$ was added to the solution at a temperature of 35 °C with continuous stirring for 1 h. Afterward, both H_2O_2 and distilled water were added to the mixture with continuous stirring for 30 min to get a brownish-yellow color of GO. The GO is separated by filtration, double washed with distilled water and dried at 70 °C for an hour. The doping process was done through dissolving one gram of GO in 50 ml of ethanol with stirring, and then the solution is subjected to sonication for 30 min. Afterward, Co and Ni acetate (with a proper mass) was added to the solution and boiled under reflux to 100 °C for 10 h. Finally, filtration is necessary to collect the solid product. To incorporate the TiO_2, the doped

GO is suspended in 15 ml of ethanol and stirred at 100 rpm a 70 °C. Then, a suitable mass of the titanium isopropoxide as a precursor of TiO_2 is added with continuous stirring until the solution loses most of the ethanol. Afterward, the mixture is placed in a furnace under vacuum at 800°C for three hours. In these experiments, the mass of GO and transition metal was fixed, and the mass of TiO_2 nanoparticles varies in such a way that the mass ratio is (GO: Ni/Co: TiO_2 = 10: 1: (1 to 5))

Characterization

To verify the doping and incorporating processes, TEM images have been captured by JEOL JEM 2010 transmission electron microscope (TEM), operating at 200 kV, (JEOL Ltd., Japan). Analysis of TEM images has been done by ImageJ 1.47v™ software. To detect the phase and crystallinity of the prepared nanocatalyst, the analysis is done by X-ray diffraction (Rigaku Co, Japan) with CuKα (λ = 1.54056 Å) radiation at a scan rate of 0.05°s⁻¹over a range of 2θ angles from 5 to 80°. The absorption spectra of the photocatalyst were investigated by spectroscopic analysis using Agilent HP 8453 UV-visible spectroscopy system, Germany. In addition, the p-CoO(GO)/n-TiO_2sample was analyzed by X-ray Microanalysis using TEAM™ EDS Analysis provided by EDAX (the operating conditions are: accelerating voltage 30 kV, current 8nA, beam diameter 6 μm, decreased vacuum in the chamber with the pressure of 50 Pa).

Application as a photocatalyst

The hydrogen production experiment has been conducted for each nanocomposite separately. At the start, 50 mg of the catalyst was added to 50 ml of solution mixture of water and methanol (4:1, v:v) in pre-purged sealed container. The gas collected from the opening and accumulates in a simple inverted graduated cylinder. From the observation of the displacement of water in the graduated cylinder with time, the volume of the gas can be calculated and The produced was determined with time intervals by hydrogen sensor. In each run, a magnetic stirrer is used to agitate the solution to reduce the hydrodynamic barrier of gas evolution during the photocatalytic reaction. The experiments have been done under solar irradiation from 12:00 ~ 13:00 in July 2018 in MiniaCity, Egypt. (Latitude: 28° 06' 35.6" N Longitude: 30° 45' 1.1" E). The experiments have been done in consecutive days and fixed time to diminish the effect of fluctuation of solar radiation. Basically, the photocatalytic water

splitting reaction produces one-third oxygen gas and two-thirds hydrogen gas. M. S. Mahmoud et al. [11] indicated experimentally that the hydrogen gas comes from water and ethanol. Moreover, they proved experimentally that CO_2 gas is not generated by collecting the evolved gases above $Ca(OH)_2$ solution, where no turbidity is observed.

Results and Discussion

Characterizations of the nanocomposite

Figure 1 (a) shows the TEM image of the prepared n-TiO$_2$@p-CoO/GO. It was evident that the GO sheet appears with small, scattered dots for Co and/or TiO$_2$ nanoparticles with an average outer diameter of ca. 52 nm. Moreover, the image shows a relatively random distribution of the nanoparticles inside the GO sheet, which can generate a local active site and facilitate the photocatalytic reaction. Figure 1 (b) shows the TEM image of n-TiO$_2$/p-NiO/GO. The appearance of black scattered dots inside GO sheet is evident. The diameter of dots is nanosized of 12 nm. TiO$_2$@NiO-GO composite showed lower sized nanoparticle thant that of TiO$_2$@CoO-GO composite, that could affect the photocatalytic activity of nanocomposite.

Subsequently, the crystal structure of the nanocomposite is confirmed by the XRD analysis. Figure 2 shows the XRD pattern of the Co/Ni-doped GO incorporated titania nanoparticles in comparison with the pure GO sample. For GO, the XRD pattern of GO shows a broad peak at 2θ of 10.1 ° (002) with an inter-layer space of ~0.34 nm and as well strong diffraction peak is located at 2θ= 24.7°). For the prepared samples, the observed broad and noise peaks could be related to the nature of the incorporation action of Co/Ni-doped GO and TiO$_2$ nanoparticles. Besides, GO peaks is probably shifted, indicating the effect of doping and incorporation on the crystal structure and morphology of the GO layer. The existence of diffraction peaks at 2 values of 9.8 °, 24.2 °, 27.8 °, 33.8 °, and 48.2 ° matching with the crystal planes of (200), (110), (310), (301), and (020) of titania nanoparticles (JCPDS card no 27-0124). For Co sample, small peaks appear at 2 values 44.2 ° and 51.5 ° matching with Co crystal planes of (002) and (101), respectively (JCPDS 05-0727). Such peaks prove the appearance of Co in the crystal structure of the GO. A similar finding is extended to the Ni sample, where a small peak at 2 values 37 ° and 34.5 ° matching with Ni crystal planes of (111) and (200), respectively (JCPDS 04-850). It is worthy mentioned that the intensity of the peaks of the prepared sample is lower than that of the pure titania nanoparticles indication the low crystallite size. Furthermore, incorporating Co or Ni doped GO with TiO$_2$ material induces the formation of smaller crystallites and decrease of crystallinity [7].

In quest of estimating the visible light absorption of the prepared samples compared to pure TiO$_2$, Fig. 3 shows the UV-vis absorption
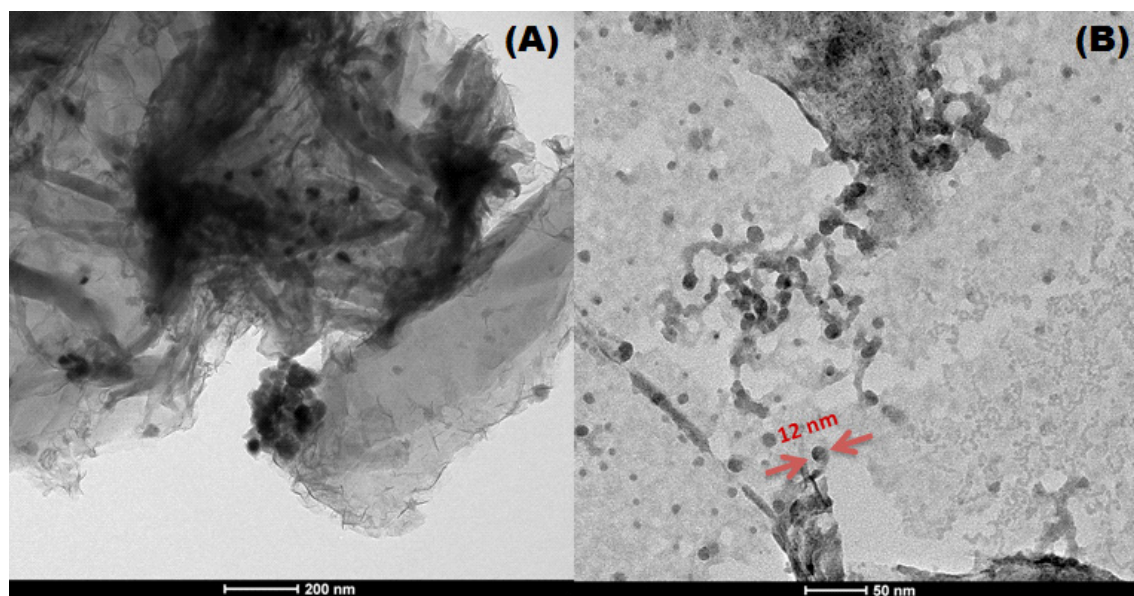

Fig. 1. TEM image of: (a)TiO2@CoO-doped GO nanoparticles (GO:Co:TiO2= 10: 1: 1), (b) TiO2@NiO-doped GO (GO:Ni:TiO2= 10: 1: 1).
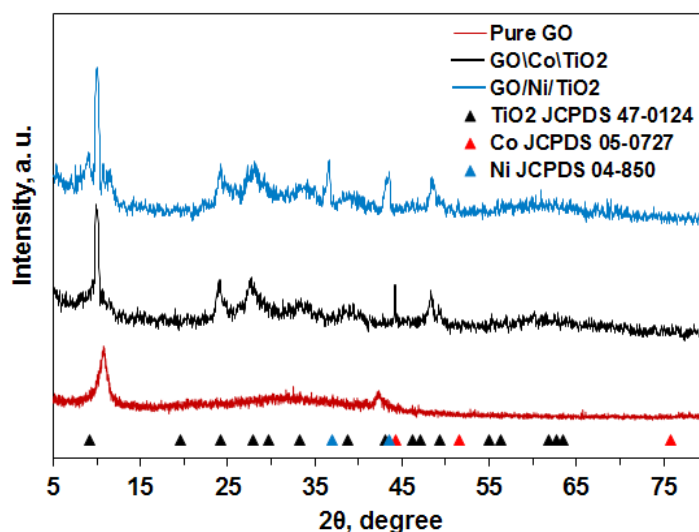
Fig. 2. The XRD patterns of the (Co/Ni)-doped GO incorporated Titania nanoparticles compared with pure GO, TiO$_2$, Ni element, and Co element.

spectra of the GO, titania (anatase), and Co/Ni-doped GO incorporated with titania nanoparticles. The fundamental absorption edge (λ_{abs}) for TiO$_2$ anatase nanoparticles can be observed at 385 nm, which corresponds to the bandgap of 3.2 eV [12]. The major absorption region for the pure anatase is in the UV region at about 385 nm. By comparing the spectrum of pure anatase and TiO$_2$@CoO-doped GO and TiO$_2$@NiO-doped GO, it is clear that introducing of CoO and NiO to composites broadened the absorption edge of the GO and TiO$_2$ that is shifted to the visible region. With reference to the solar spectrum in the visible region (100%), the absorption of visible radiation has increased to 39.8% and 62.3% for TiO$_2$@CoO-doped GO and TiO$_2$@NiO-doped GO samples, respectively. This finding can be considered as a potential reason for the improved performance of the TiO$_2$@CoO-doped GO and TiO$_2$@NiO-doped GO nanocomposites compared to both the GO and pure TiO$_2$. Mathematically, the direct bandgap of the prepared nanocomposites can be calculated using the following equation [13]:

$$(\alpha h v) = A(h v - E_g)^{n/2} \qquad \text{Eq (1)}$$

Where α is the absorption coefficient, h is the Planck constant, v is the photon frequency ($h v = 1240$/wavelength), A is the proportionality constant, Eg is the bandgap, and n is a constant. Different values of n are assumed according to whether the bandgap is direct or indirect. It takes

a value of $n= 1$ for indirect allowed and $n= 4$ for the direct allowed absorption according to the optical transition type of the photocatalyst. The inset of Fig. 3 shows the plot of $(\alpha h v)^2$ versus photon energy at $n=4$ (direct allowed bandgap). It was showed that the bandgap values of Co TiO$_2$@CoO-doped GO and TiO$_2$@NiO-doped GO nanoparticles are 2.72, 2.6 eV, respectively. This indicated that the bandgap energies for TiO$_2$@CoO-doped GO and TiO$_2$@NiO-doped GO are lower than that of anatase TiO$_2$. This finding is agreement with previously stated [14]. It was presence of transition the p-type metal oxide on GO sheet forms a heterojunction with n-type TiO$_2$ which generates the synergistic effect via promoting the extension of electron/hole lifetime due to difference Fermi levels.

In order to determine the atomic composition of the samples, the EDX analysis has conducted to p-CoO(GO)/n-TiO$_2$. Figure 4 shows the EDS analysis of the sample. It is evidence that the report shows the appearance of C, Ti, and Co with atomic % of 67.91, 23.89 and 3.48 %, respectively. However, this data misjudge the exact percentage of oxygen attached to both carbon and titanium atoms due to the nature of EDS analysis, which works only for a thin layer (few microns or less) on the surface.

Photo-catalytic activity study
Figure 5(a) displays the volume of hydrogen generated as a function of time for different ratios
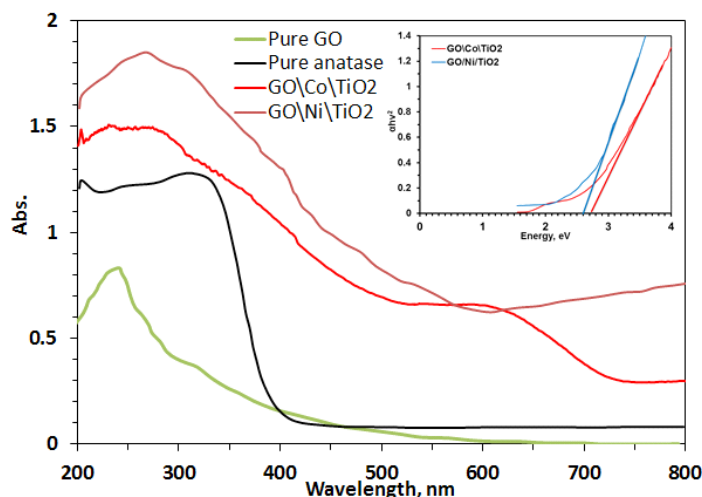
Fig. 3. UV-visible absorbance spectra for pure anatase, GO, and Co/Ni- doped GO incorporated Titania nanoparticles (GO: Co (or Ni): TiO$_2$= 10:1:1). Inset: Tauc plot for calculation of direct bandgap energies of Co/Ni- doped GO incorporated Titania nanoparticles.
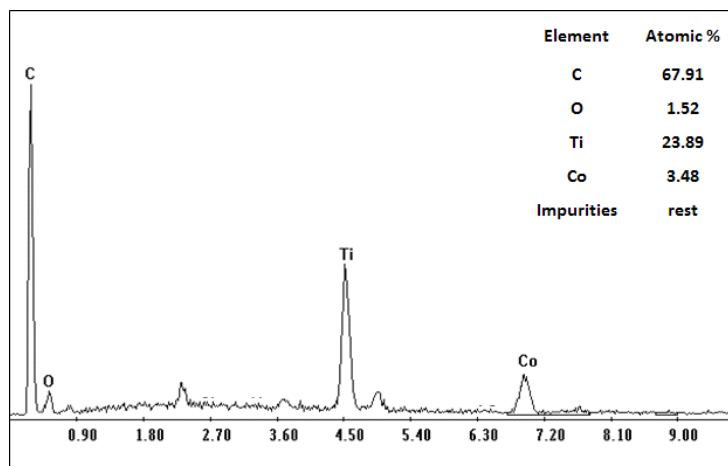

Element	Atomic %
C	67.91
O	1.52
Ti	23.89
Co	3.48
Impurities	rest

Fig. 4. The EDS ofCo-doped GO incorporated Titania nanoparticles

of n-TiO$_2$/p-NiO/GO. It is clear that the ratio of GO: Ni: TiO$_2$= 10:1:2 provided a comparatively better evolution rate of 150 μmol H$_2$/min. More introduction of TiO$_2$ nanoparticles showed a less rate of hydrogen production. Moreover, Fig. 5(b) shows the volume of hydrogen generated vs. time for different ratios of Co-doped GO and TiO$_2$ nanoparticles. It is evident that the best ratio of GO: Co: TiO$_2$ was 10:1:5, which induced an average rate of hydrogen reduction of 62.5 μmol H$_2$/min.

A comparison between the GO, TiO$_2$ nanoparticles, and the two types of photocatalysts is shown in Fig. 5(c). It is clear that n-TiO$_2$@p-NiO/GO has the highest rate of hydrogen production (150 μmol H$_2$ g$_{catalyst}^{-1}$. min^{-1}). It was worthy noted that hydrogen production rate of n-TiO$_2$@p-NiO/GO is 2.4 fold higher than that of n-TiO$_2$@p-CoO/GO (62.5 μmol H$_2$ g$_{catalyst}^{-1}$. min^{-1}) and 5 folds higher than that of TiO$_2$ nanoparticles (30 μmol H$_2$ g$_{catalyst}^{-1}$. min^{-1}).

The theoretical number of electrons in the conduction band of a semiconductor is given by [27]:

$$N_{cb} = AT^{3/2} e^{-E_{gap}/2kT} \qquad \text{Eq (2)}$$

where A is constant = 4.83×10^{21} (electronsm^{-3} K$^{-3/2}$), E_{gap} is the bandgap energy (eV), k is the Boltzmann constant, and T is the temperature (~303 K). For n-TiO$_2$/p-NiO/GO, the value of

N_{cb} = 0.6229×10^4 electrons. m^{-3} (11.212×10^3 electrons. g$_{catalyst}^{-1}$)

It has been reported formerly that both NiO and CoO are p-type while TiO$_2$ is n-type semiconductor [15-17]. The bandgap of NiO, CoO, and TiO$_2$ are 2.6, 2.6 and 3.2 eV, respectively as shown in Table 1.

The n-type TiO2 provides more electrons that can easily transfer to the conduction band, as the energy level between the donor and the conduction band is low. They tend to form more levels above the Fermi level, thus skewing the electron distribution higher.

The inner electric field generated by the p-n junction region efficiently transferred the photogenerated holes into VB band of NiO or CoO and the photogenerated electron transfer into the conduction band of TiO2 as well. Subsequently, recombination of photogenerated electron-hole pairs was constrained [3]. The photogenerated electrons were involved in reduction reactions of water into H2.

Accordingly, the coupling of TiO2 with GO doped with NiO and CoO results in; i) Improve the visible light absorption ii) Enhance the electron/hole separation iii) Prolong the recombination of the electron/hole charge carrier. The main enhancement mechanism for the charge transfer step is achieved through the electron transfer through the interface between the base and dopant metal oxides. This can be clarified by the development of an inner electric field, which thus impedes the electron/gap recombination activity [18].

GO has a significant effect on enhancing H2 production via i) facilitating the electron mobility ii) promotes the electron injection into the conduction band of the Ni and Co dopant iii) acting as a photocathode site for hydrogen evolution reaction due to the presence of π*-orbitals.

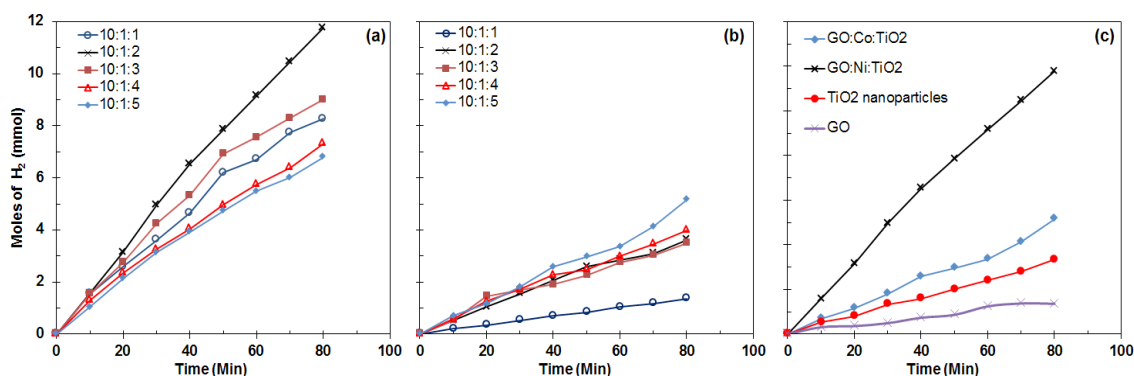In case of p-NiO(GO)/n-TiO$_2$, both band gaps

Fig. 5. (a) The hydrogen specific evolution as a function of time for different Ni-doped GO incorporated Titania nanoparticles, (b) The hydrogen specific evolution as a function of time for different Co-doped GO incorporated Titania nanoparticles. (c) A comparison between the hydrogen evolution using pure Titania nanoparticles, pure GO, and for the top results obtained by using both Ni and Co- doped GO incorporated Titania nanoparticles.

TABLE 1. The VB and CB levels of appearing oxides.

Semiconductor	Levels of bands versus NHE in eV			Ref.
	CB	VB	Eg	
TiO$_2$ (Anatase)	-0.25	2.95	3.2	[19]
NiO	-1.5	4.1	2.6	[20]
CoO	-1	1.6	2.6	[18]
GO	-0.75	1.55	2.3	[15]

of NiO and TiO$_2$ are 2.6 and 3.2 eV, respectively. Furthermore, at the interface between NiO and TiO$_2$, a space charge region will build up due to the formation of *p-n* heterojunction result in a localized electrical field between NiO and TiO$_2$ [21]. Consequently, the generated e⁻/h⁺ pairs in the TiO$_2$ due to UV light irradiation will be maintained through the effect of the electric field formed by the p-NiO/n-TiO$_2$ heterojunction as shown in Fig. 6. The photon-induced holes in the TiO$_2$ transferred NiO. Therefore, the charge separation is taken place preventing recombinatrion that results in forward of photocatalysis reaction of H$_2$ generation. As well, the expected lifetime of e/h pair is considerably prolonged as a result of the inhibition of their recombination. Accordingly, the rate of hydrogen evolution reaction is increased. As well, in p-CoO/ n-TiO$_2$ heterojunction, the generated e⁻/h⁺ pairs of TiO$_2$ particle upon light irradiation will be maintained through the effect of the electric field formed by the p-CoO/n-TiO$_2$ heterojunction as shown in Fig. 6 Meanwhile, p-CoO has lower negative CB potential energy than that of NiO, thus, the probability of inhibition of charge recombination of p-NiO/n-TiO$_2$ is higher that p-CoO/n-TiO$_2$ heterojunction. Therefor, higher improving of the photcatalytic H$_2$ production rate of TiO$_2$@NiO/ GO was achieved rather than TiO$_2$@CoO/ GO. This is attributed to TiO$_2$@NiO-GO composite nanoparticle size (12 nm) is 4 folds lower than that of TiO$_2$@CoO-GO composite, thus another effect of quantum effect was involved in improving the photocatalytic activity of TiO$_2$@NiO/ GO nanocomposite. Previously, doping of TiO$_2$ with metals improved the photocatalystic actvity via suppressing the recombination of photogenerated

holes and electrons[23,24].

Generally, the performance of a photocatalyst is obtained by calculating the efficiency of conversion of photons to electrons as follows:

$$\eta = \frac{N_{electrons}}{N_{photons}} \qquad \text{Eq (3)}$$

Where, $N_{electrons}$ is the number of electrons involved in the photo-reduction reaction, and $N_{photons}$ is the number of photons incident in the reaction area. The $N_{electrons}$ can be obtained from the rate of hydrogen generation form Fig. 5 (for n-TiO$_2$/p-NiO/GO = 150 µmol H$_2$ g$_{catalyst}^{-1}$ min^{-1}). This rate provides the number of electrons involved in hydrogen evolution step. Similarly, $N_{photons}$ can be calculated from:

$$N_{photons} = \frac{I \, [J \, s^{-1}]}{E_{photons} \, [J \, photon^{-1}]} \qquad \text{Eq (4)}$$

Where I is the solar intensity in Js^{-1} (258-266.7 Wm^{-2}) [25], and $E_{photons}$ is the photon energy (3.97×10^{-19} in J photon^{-1}). Therefore, the photon flux is 6.506 × 10^{20} photons/s m^2 solar. This calculation shows that the prepared catalyst has achieved approximately 3.11 % conversion of photons to electrons. Although it is a small conversion percentage, it indicates that this photocatalyst focuses on increasing the absorbance of photons and providing prolonged time for more water molecules to be photo-oxidized.

For comparison the obtained results with related works, Table 2 shows the rate of hydrogen evolution for various types of photocatalysts. It is noticed that the rate of hydrogen production
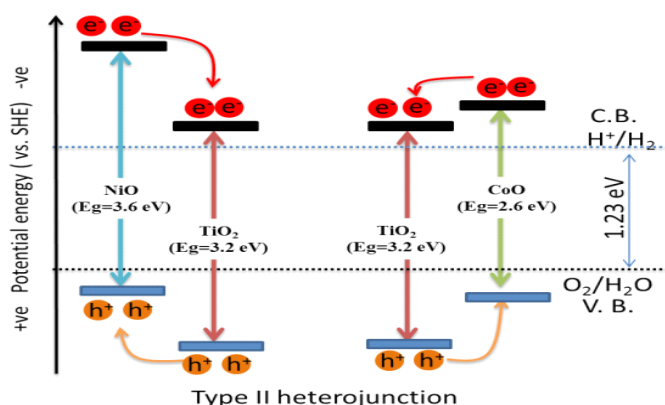

Fig. 6. Proposed mechanism for photocatalytic water splitting by Ni/Co-doped GO incorporated Titania nanoparticles.

by Fe/Co-Titania nanotube is higher than that previously obtained [32,33]. This reveals that the n-TiO$_2$/p-NiO/GO nanoparticles could be a promising photocatalyst candidate in the photon-induced water splitting reaction. But, the stability of the photocatalyst should be examined well before claiming its effectiveness.

Conclusion

The preparation and characterization of p-n junction by incorporating p CoO/NiO doped GO with n-TiO$_2$ nanoparticles has been investigated. TEM images showed the appearance of small, scattered dots for Co, Ni and TiO$_2$ nanoparticles within the GO sheet. TEM shows a relatively random distribution of the nanoparticles inside the GO sheet with quantum dot sized NiO. XRD patterns showed the existence of diffraction peaks that verifies the presence of the TiO$_2$, Co, and Ni nanoparticles. The EDS analysis confirmed the presence of cobalt, carbon, oxygen, and titanium in the sample. n-TiO$_2$@p-NiO/GO photocatalyst showed a hydrogen evolution rate of 150 that is higher than that of n-TiO$_2$@p-CoO/GO; 61 µmol H$_2$ g$_{catalyst}$$^{-1}$ min^{-1}. p-NiO/n-TiO$_2$ heterojunction showed better activity than p-CoO/n-TiO$_2$ due to more negativity of CB of p-NiO than that of p-CoO. Accordingly, the two nanocomposites showed good photocatalytic activity toward water splitting under the visible light irradiation, which was concluded by the distinct increase in the hydrogen evolution rate compared to the TiO$_2$.

TABLE 2. A comparison of the hydrogen evolution rate for different nanocatalysts

Type of photocatalyst	Initial rate of hydrogen evolution	Ref.
Graphene sheet @TiO$_2$	12.27 µmolg^{-1} min^{-1}	[26]
r-CD/Pt	11.4 µmolH$_2$ g^{-1} min^{-1}	[27]
Pt/TiO$_2$ nanosheet	5.6 µmolH$_2$ g^{-1} min^{-1}	[28]
TiO$_2$	100 µmol H$_2$ g^{-1} min^{-1}	[29]
ZnIn$_2$S$_4$	25.75 µmol H$_2$ g^{-1} min^{-1}	[30]
Graphene /Ni(OH)$_2$	1.83 µmol H$_2$ g^{-1} min^{-1}	[31]
Ag$_3$PO$_4$-TiO$_2$-Graphene Oxide	3.67 µmol H$_2$ g^{-1} min^{-1}	[32]
MoS$_2$/Graphene Oxide	7.5 µmol H$_2$ g^{-1} min^{-1}	[33]
TiO$_2$@NiO -GO nanoparticles	150 µmol H$_2$ g$_{catalyst}$$^{-1}$ min^{-1}	Current study
TiO$_2$@NiO -GO nanoparticles	62.5 µmol H$_2$ g$_{catalyst}$$^{-1}$ min^{-1}	Current study

References

1. Badawy M.I., Ali M.E.M., Ghaly M. Y., El-Missiry M.A.. Mesoporous simonkolleite–TiO2 nanostructured composite for simultaneous photocatalytic hydrogen production and dye decontamination, *Process Safety and Environmental Protection* **94**, 11–17 (2015).

2. Badawy M. I., Ghaly M. Y, Ali M. E.M., Photocatalytic Hydrogen Production over Nano-structured Mesoporous Titania from Olive Mill Wastewater. *Desalination*, **267** (2-3), 250-255 (2011).

3. Ali M. E. M, Alhathal Alanezi A, Azeez FA, Ghaly MY, Photoassisted mineralization of remazole red F3B over NiO/TiO2 and CdO/TiO2 nanoparticles under simulated sunlight, *Separation Science and Technology* **53** (1), 170-180 (2018).

4. N.A. Barakat, A. Taha, M. Motlak, M. Nassar, M. Mahmoud, S.S. Al-Deyab, M. El-Newehy, H.Y. Kim, ZnO&Fe2O3-incorporated TiO2 nanofibers as super effective photocatalyst for water splitting under visible light radiation, *Appl. Catal. A*, **481**, 19-26 (2014).

5. Bak T., Nowotny J., Rekas M., Sorrell C., Photo-

electrochemical hydrogen generation from water using solar energy. Materials-related aspects, *Int. J. Hydrogen Energy,* **27**, 991-1022 (2002).

6. Ismail A. A., Mesoporous PdO–TiO2 nanocomposites with enhanced photo-catalytic activity. *Appl Catal, B: Environ,* **117-118**, 67-72 (2012).

7. Zhao X., Cai Z., Wang T., O'Reilly SE., Liu W., Zhao D, A new type of cobalt-deposited titanate nanotubes for enhanced photocatalytic degradation of phenanthrene, *Appl Catal B: Environ.,* **187**, 134-143 (2016).

8. Khalid N. R., Ahmed E., Zhanglian H., Zhang Y., Ahmed M. M.. Graphene modified Nd/TiO2 photo-catalyst for methyl orange degradation under visible light irradiation. *Ceram Int;* **39**, 3569-3575 (2013).

9. Hyunwoong P., Yiseul P., Wooyul K., Wonyong C.. Surface modification of TiO2 photo catalyst for environmental applications. *J. Photochem Photobiol* **C**, 1-20 (2012).

10. Xue J.   , Jawad N., Biswarup P., Jijun Z.   , A. Rajeev. Graphene oxide as a chemically tunable 2-D material for visible-light photo-catalyst applications. *J. Catal,* **299,** 204-209 (2013).

11. Mahmoud M. S. , Ahmed E. , Farghali A. A. , Zaki A. H. , Abdelghani E. A. M. , Barakat N. A. M., Influence of Mn, Cu, and Cd–doping for titanium oxide nanotubes on the photocatalytic activity toward water splitting under visible light irradiation, *Colloids Surf A Physicochem Eng Asp,* **554** (5), 100-109 (2018).

12. Muniyappan S., T. Solaiyammal, K. Sudhakar, A. Karthigeyan, P. Murugakoothan, Conventional hydrothermal synthesis of titanate nanotubes: Systematic discussions on structural, optical, thermal and morphological properties, *Modern Electronic Materials* (2017).

13. Momeni M. M., Ghayeb Y., Visible light-driven photoelectrochemical water splitting on ZnO–TiO2 heterogeneous nanotube photoanodes, *J. Appl. Electrochem.,* **45**, 557-566 (2015).

14. Yeha T., Teng H., Graphite oxide with different oxygen contents as photocatalysts for hydrogen and oxygen evolution from water, *ECS Transactions,* **41** (40), 7-26 (2012).

15. Munawar K., Mansoor M. A., W. J. Basirun, M. Misran, N. M. Huang, M. Mazhar, Single step fabrication of CuO–MnO–2TiO2 composite thin films with improved photoelectrochemical

16. Irwin M. D., Buchholz D. B., Hains A. W., Chang R. P. H., Marks T. J., P-type semiconducting nickel oxide as an efficiency-enhancing anode interfacial layer in polymer bulk-heterojunction solar cells, *Proc Natl Acad Sci U S A.,* **105** (8), 2783-2787 (2008).

17. Ramakrishnan V., Hyun K., Park J. and Yang B. L., Cobalt oxide nanoparticles on TiO2 nanorod/ FTO as a photoanode with enhanced visible light sensitization, *RSC Adv.*, 1-3 (2015).

18. Tamirat G., Rick J., Dubale A. A., Su W. N., Hwang B. J., Using hematite for photoelectrochemical water splitting: a review of current progress and challenges, *Nanoscale Horiz,* **1**, 243-267 (2016).

19. Echresh, Abbasi M. A., Shoushtari M. Z., Farbod M., Nur O., Willander M., Optimization and characterization of NiO thin film and the influence of thickness on the electrical properties of n-ZnO nanorods/p-NiO heterojunction, *Semicond. Sci. Technol,* **29** (11), 115009 (2014).

20. Lin Y. H., Wu Y. C., Lai B. Y., Collection efficiency enhancement of injected electrons in dye-sensitized solar cells with a Ti interfacial layer and TiCl4 treatment. *Int. J. Electrochem. Sci.,* **7**, 9478-9487 (2012).

21. Low J., Yu J., Jaroniec M., Wageh S., Al□Ghamdi A.A., Heterojunction photocatalysts, *Adv. Mater.,* **29**, (2017). doi: 10.1002/adma.201601694

22. Li R. Z. , J Liang. , Xu X. L. , Xu H. G. , Zheng W. J. , Photoelectron spectroscopy and density functional theory study of ConO- (n=1-3), *Chem. Phys. Lett.,* **575**, 12-17 (2013).

23. Hanna A. A., Mohamed W.A.A., Ibrahim I.A.. Studies on Photodegradation of Methylene Blue (MB) by Nano-sized Titanium Oxide, *Egy. J. Chem.,* **57**(4), 315-325 (2014).

24. El Nazer H.A., EL-Rafei A.M., Preparation of Photoactive Tungsten-doped Anatase Nanotubes Using Hydrothermal Technique. *Egy. J. Chem.,* **59** (6), 955-966 (2016).

25. Bady M., Towards Sustainable Power Generation Using Solar Chimney, *OALib Journal,* **21**, (2015).

26. Xiang Q. J., Yu J. G., Jaroniec M., Enhanced photocatalytic H2-production activity of graphene-modified titania nanosheets, *Nanoscale,* **3**, 3670(2011).

27. X. Xu, W. Tang, Y. Zhou, Z. Bao, Y. Su, J. Hu, H. Zeng, Steering photoelectrons excited in carbon dots into platinum cluster catalyst for solar-driven hydrogen production, *Adv. Sci.,* 1700273-1700279 (2017).

28. Yu J., Qi L., Jaroniec M., Hydrogen production by photocatalytic water splitting over Pt/TiO2 nanosheets with exposed (001) facets, *J. Phys. Chem. C,* **114**, 13118-13125 (2010).

29. Zhang Y., Xia T., Shang M., Wallenmeyer P., Katelyn D., Peterson A., Murowchick J., Dong L., Chen X., Structural evolution from TiO2 nanoparticles to nanosheets and their photocatalytic performance in hydrogen generation and environmental pollution removal, *RSC Adv.,* **4**, 16146-16152(2014).

30. Bai X., Li J., Structural and microstructural investigation of CdxZn1-xIn2S4 photocatalyst for solar hydrogen production, *Mater. Res. Bull,* **46**, 1028-1034 (2012).

31. Oliva J., Gomez-Solis C., Diaz-Torres L. A., Martinez-Luevanos A., Martinez A. I., and Coutino-Gonzalez E., Photocatalytic hydrogen evolution by flexible graphene composites decorated with Ni(OH)2 nanoparticles, *J. Phys. Chem. C*, **122**, 1477-1485(2018).

32. Sheu F., Cho C., Liao Y., Yu C., Ag3PO4-TiO2-graphene oxide ternary composites with efficient photodegradation, hydrogen evolution, and antibacterial properties, *Catalysts*, **8**, 57 (2018).

33. Wang M., Han X., Zhao Y., Li J., Ju P., Hao Z., Tuning size of MoS2 in MoS2/graphene oxide heterostructures for enhanced photocatalytic hydrogen evolution, *J. Mater Sci,* **53**, 3603(2018).

متراكبات نانومترية من اكسيد التنانيوم المطعم من النيكل او الكوبالت و الجرافين لإنتاج الهيدورجين

محمد المطيري[1]، ابراهيم اسماعيل ابراهيم[2]، محمد صلاح محمود[2,3]، محمد شعبان عتريس[4]، محمد عيد محمد علي [5]، ياسر خواص[5]

[1]وزارة الكهرباء و المياه ، الكويت ، الكويت ص.ب 120120
[2]الهندسة الكيميائية- جامعة المنيا - المنيا- مصر - ص.ب 61111
[3]كلية العلوم التطبيقية - قسم الهنسدسة - سحار - سلطنة عمان ص.ب 311
[4]هسئة المواد النووية - طريق المعادي - القطامية - القاهرة - مصر ص.ب 530
[5]قسم بحوث تلوث المياه - شعبة بحوث البيئة - المركز القومي للبحوث - الدقي - القاهرة مصر ص. ب 12622

تم تحضير متراكبات نانومترية من اكسيد التنانيوم المطعم من النيكل او الكوبالت و الجرافين بنجاح و للاستخدام في تكسير المياه لإنتاج الهيدورجين. تم توصيف المواد المحضره بطرق مختلفة و اظهرت صور الميكروسكوب الالكتروني الناقل تواجد نقاط ضغيرة من الكوبالت و اكسيد النتانيوم متناثرة على سطح الجرافين. اظهرت نتائج كفاءة عالية في انتاج الهيدورجين على سطح من اكسيد التنانيوم/الجرافين المطعم من النيكل من 0.3 مليمول هيدورجين لكل دقيقة لكل اجرام من العامل الحافز و اكثر كفاءة من اكسيد التنانيوم/الجرافين المطعم من الكوبالت. الكفاءة العالية في انتاج الهيدورجين نابع من القدرة على فصل الشحنات و ايضا قلة طاقة التنشيط الضوئي.